# Bethe-Heitler pair production in ultrastrong short laser pulses

K. Krajewska,[1] C. Müller,[2,3] and J. Z. Kamiński[1]

[1]*Institute of Theoretical Physics, Faculty of Physics, University of Warsaw, Hoża 69, 00-681 Warsaw, Poland*

[2]*Institut für Theoretische Physik, Heinrich-Heine-Universität Düsseldorf, D-40225 Düsseldorf, Germany*

[3]*Max-Planck-Institut für Kernphysik, Saupfercheckweg 1, 69117 Heidelberg, Germany*

(Received 12 April 2013; published 13 June 2013)

Production of electron-positron pairs from vacuum in the combined electromagnetic fields of a high-intensity laser pulse and an atomic nucleus is studied within the framework of laser-dressed quantum electrodynamics. The focus lies on the influence exerted by a finite laser pulse length on the energy spectra of created electrons and positrons, which is examined in a broad range of field frequencies and intensities. The results for an isolated short laser pulse are also compared with corresponding calculations for an infinite train of laser pulses. It is shown that the laser pulse length and its carrier-envelope phase have a substantial effect on the pair creation process, leading to both quantitative and qualitative differences in the particle spectra.

DOI: 10.1103/PhysRevA.87.062107 PACS number(s): 12.20.Ds, 34.50.Rk, 32.80.Wr

## I. INTRODUCTION

Investigations of electron-positron ($e^-e^+$) pair production via multiphoton absorption in the strong electromagnetic fields of intense laser radiation started in the 1960s [1–3]. While the problem was of purely theoretical interest at that time, nowadays there is a clear perspective for corresponding experimental studies due to a remarkable and still ongoing progress in high-power laser technology. Field intensities well beyond $10^{20}$ W/cm$^2$ are available today in many laboratories worldwide and an increase towards $10^{25}$ W/cm$^2$ is envisaged within the Extreme Light Infrastructure (ELI) project [4]. This way the characteristic intensity level for extracting $e^-e^+$ pairs out of the vacuum, given by the critical value $I_{\rm cr} \sim 10^{29}$ W/cm$^2$, is being approached. These developments have stimulated substantial theoretical activities on $e^-e^+$ pair production and other quantum electrodynamic processes in high-intensity laser fields during the last decade [5,6].

Already at present, a suitable combination of advanced technologies allows for experimental studies on $e^-e^+$ pair production in strong laser fields. The relevant field intensity can be amplified effectively when a highly relativistic particle beam from an accelerator counterpropagates an intense laser pulse. In the rest frame of the projectile particles the laser intensity is enhanced by a factor $4\gamma^2$ where $\gamma \gg 1$ denotes the relativistic Lorentz factor. In this manner the first (and so far only) observation of $e^-e^+$ pair production via multiphoton absorption was accomplished in ultrarelativistic electron-laser collisions at the Stanford Linear Accelerator Center (SLAC) in the 1990s [7]. The detected pairs were attributed to a multiphoton version of the Breit-Wheeler process, according to $\omega_{\rm C} + N\omega_{\rm L} \to e^-e^+$, with a high-energy photon $\omega_{\rm C}$ generated through Compton backscattering and a certain number $N$ of laser photons $\omega_{\rm L}$ being involved.

Another mechanism of laser-induced $e^-e^+$ pair production is the nonlinear Bethe-Heitler process, $Z + N\omega_{\rm L} \to Z + e^-e^+$, where the leptons are created by laser radiation in the vicinity of an atomic nucleus. This is the subject of the present paper. This hitherto unobserved process could, in principle, be realized by exploiting the relativistic nuclear beams ($\gamma \sim 10^3$–$10^4$) of the Large Hadron Collider at CERN, together with superstrong laser beams of intensity $10^{22}$ W/cm$^2$. At the future ELI facility, corresponding measurements could be conducted at significantly lower nuclear beam energies ($\gamma \sim$ 10–100). In view of these prospects, it is important to develop more and more refined theoretical models in order to provide a realistic description of the experimental situation.

Various aspects of nonlinear Bethe-Heitler pair production in relativistic nucleus-laser collisions have already been studied theoretically. Total production rates and positron or electron spectra were obtained in a broad range of field parameters [8–13]. The relevance of bound atomic states [14], the influence of nuclear recoil [15–18], and electron spin effects [19,20] have also been explored. Besides, Bethe-Heitler pair production in a combination of high-frequency and low-frequency laser fields was studied [21,22]. Very recently, the process has been calculated in a bichromatic laser field of commensurate frequencies, revealing quantum interference and relative phase effects [23,24]. In all these investigations the laser field was assumed to be of infinite extent in space and time.

In the present paper, we consider $e^-e^+$ pair production via the nonlinear Bethe-Heitler process in a laser pulse of finite length. Our study is motivated by the fact that laser fields of ultrahigh intensity, as required for pair production, are typically generated in short pulses comprising just a few field oscillations. We generalize the well-established theory based on Dirac-Volkov states to the case where the laser field is nonzero only on a finite phase interval. Our theory enables us to treat nonlinear Bethe-Heitler pair production by single laser pulses of arbitrary length. In particular, the case of a very short few-cycle pulse will be investigated in detail. We also compare our results for a single laser pulse with the periodic situation of an infinite train of pulses. It will be shown that the precise shape of the laser field exhibits a characteristic influence on the electron and positron energy spectra. Our study complements earlier calculations where nonlinear Bethe-Heitler pair production in a finite, but relatively long laser pulse (comprising many field oscillations) was analyzed [25]. Besides, the process was also considered for a pulse train of special form which can be modeled within a bichromatic theory [23].

We point out that calculations of quantum electrodynamical processes in finite laser pulses have recently been performed

 

with regard to nonlinear Compton scattering [26–31] and nonlinear Breit-Wheeler pair production [32–34]. Both reactions are related via a crossing symmetry of the corresponding Feynman graphs. The latter process offers moreover an interesting means to measure the duration of ultrashort high-energy photon pulses [35]. Also other mechanisms of laser-induced $e^-e^+$ pair creation involving short field pulses or special field combinations have been examined (see, e.g., Refs. [36–43]). In addition we note that $e^-e^+$ pairs can be produced very efficiently through interaction of high-intensity laser pulses with solid targets. Here the pair production relies on a reaction chain, with the ordinary (linear) Bethe-Heitler effect representing the final step [44].

It is well known that laser-induced $e^-e^+$ pair production shares characteristic similarities with atomic ionization in strong laser fields [45]. In our study we shall mainly focus on a nonperturbative interaction regime, which corresponds to the above-threshold ionization (ATI) of atoms. Effects of ultrashort few-cycle pulses on ATI have been studied thoroughly, both in theory and experiment [46]. Relativistic ATI [47,48] and electron spin effects [49,50] were examined as well. Another analogy of field-induced pair production can be realized by interband transitions in optical lattices [51].

The paper is organized as follows. In Sec. II we present our theoretical approach to nonlinear Bethe-Heitler pair creation in a laser field of finite length. First, the case of a single, isolated laser pulse will be treated (Sec. II A) and, afterward, the case of a laser pulse train (Sec. II B). The pulse shapes under consideration are introduced in Sec. III. Results of our numerical calculations are shown and discussed in Sec. IV. Here we focus on differences in the electron and positron energy spectra when the pair creation occurs in a single pulse or a train of pulses. Pulses comprising very few or several field oscillations are considered. The resulting pair yields are compared in Sec. V. In Sec. VI we summarize the conclusions that can be drawn from our study. Some details of the calculations are provided in the Appendixes. Throughout the paper, we use the notation and mathematical convention introduced in Ref. [31].

## II. THEORY

### A. Single laser pulse

In this section, we formulate the theory for the Bethe-Heitler process by a finite laser pulse, which is similar to the approach introduced by Neville and Rohrlich in the context of Compton scattering [52]. We assume that the pulse lasts for a time $T_{\rm p}$, which defines the fundamental frequency of the laser field oscillations $\omega = 2\pi/T_{\rm p}$ and the wave four-vector $k = k^0(1,\boldsymbol{n})$, where $\omega = ck^0$. We consider a laser pulse described by the following four-vector potential,

$$A(k\cdot x) = A_0[\varepsilon_1 f_1(k\cdot x) + \varepsilon_2 f_2(k\cdot x)], \tag{1}$$

where the polarization four-vectors are such that $\varepsilon_i\cdot\varepsilon_j = -\delta_{ij}$ and $k\cdot\varepsilon_i = 0$. Without loss of generality, we assume that both polarization vectors are real, i.e., each of them is linearly polarized. However, the vector potential (1) defines an arbitrary polarized laser field, depending on the choice of the shape functions $f_i(k\cdot x)$. We will use the parameter $\mu$, which defines the strength of the laser field, $\mu = |eA_0|/(m_ec)$ with $e<0$ being the electron charge. The laser pulse shape functions $f_i(k\cdot x)$ are chosen such that the following condition is satisfied,

$$A(k\cdot x) = 0 \quad \text{for} \quad k\cdot x < 0 \quad \text{and} \quad k\cdot x > 2\pi. \tag{2}$$

For an electron (positron) that is coupled to the electromagnetic radiation (1), the Dirac equation has the form

$$(i\partial\!\!\!/ - eA\!\!\!/ - m_ec)\psi^{(\beta)}_{\boldsymbol{p},\lambda}(x) = 0, \tag{3}$$

where solutions $\psi^{(\beta)}_{\boldsymbol{p},\lambda}(x)$ are called the Volkov waves [53]. Here, the Volkov solutions are labeled by three indices; while $\boldsymbol{p}$ and $\lambda$ refer to the particle momentum outside the laser focus and to its spin projection, respectively, $\beta$ distinguishes between positive- and negative-energy states that correspond to an electron ($\beta=+1$) or to a positron ($\beta=-1$). In the most general form, these solutions are given by (see Ref. [16])

$$\psi^{(\beta)}_{\boldsymbol{p},\lambda}(x) = \sqrt{\frac{m_ec^2}{VE_{\boldsymbol{p}}}}\left(1 - \frac{\beta e}{2k\cdot p}A\!\!\!/k\!\!\!/\right)u^{(\beta)}_{\boldsymbol{p},\lambda}\, e^{-i\beta S^{(\beta)}_p(x)}, \tag{4}$$

where $u^{(\beta)}_{\boldsymbol{p},\lambda}$ are four-spinors satisfying the field-free equation, $(p\!\!\!/ - \beta m_ec)u^{(\beta)}_{\boldsymbol{p},\lambda} = 0$. These four-spinors are normalized such that $\bar{u}^{(\beta)}_{\boldsymbol{p}\lambda}u^{(\beta')}_{\boldsymbol{p}\lambda'} = \beta\delta_{\beta\beta'}\delta_{\lambda\lambda'}$. In addition, the phase factor $S^{(\beta)}_p(x)$ is

$$S^{(\beta)}_p(x) = p\cdot x + \int^{k\cdot x} d\phi\left[\beta\frac{eA(\phi)\cdot p}{k\cdot p} - \frac{e^2A^2(\phi)}{2k\cdot p}\right]. \tag{5}$$

Here, $E_{\boldsymbol{p}} = cp^0 \geqslant m_ec^2$ and $p = (p^0,\boldsymbol{p})$. Since the condition (2) is imposed, the momentum $p$ that is present in Eqs. (4) and (5) is interpreted as a field-free asymptotic momentum of a particle. Thus, it satisfies the on-shell mass relation $p\cdot p = (m_ec)^2$.

In the so-called potential approximation, the $S$-matrix amplitude describing the nonlinear Bethe-Heitler process can be written as

$$S_{\rm fi} = -iZ\alpha\int d^4x\,\frac{1}{|\boldsymbol{x}|}\left[j^{(+-)}_{\boldsymbol{p}_{e^-}\lambda_{e^-},\boldsymbol{p}_{e^+}\lambda_{e^+}}(x)\right]^0, \tag{6}$$

where $Z$ is the atomic number of an atomic nucleus, $\alpha = e^2/(4\pi\varepsilon_0c)$ is the fine structure constant and $j^{(+-)}_{\boldsymbol{p}_{e^-}\lambda_{e^-},\boldsymbol{p}_{e^+}\lambda_{e^+}}(x)$ is the electron-positron four-current with the $\nu$ component defined as

$$\left[j^{(+-)}_{\boldsymbol{p}_{e^-}\lambda_{e^-},\boldsymbol{p}_{e^+}\lambda_{e^+}}(x)\right]^\nu = \bar{\psi}^{(+)}_{\boldsymbol{p}_{e^-}\lambda_{e^-}}(x)\gamma^\nu\psi^{(-)}_{\boldsymbol{p}_{e^+}\lambda_{e^+}}(x). \tag{7}$$

Substituting here the Volkov solutions (4), the $S$-matrix amplitude (6) becomes

$$S_{\rm fi} = -iZ\alpha\frac{m_ec^2}{V\sqrt{E_{\boldsymbol{p}_{e^-}}E_{\boldsymbol{p}_{e^+}}}} \times\int d^4x\,\frac{1}{|\boldsymbol{x}|}\,\mathcal{C}^0(k\cdot x)\,e^{-iQ\cdot x - iH(k\cdot x)}, \tag{8}$$

where $Q = -p_{e^-} - p_{e^+}$, whereas

$$H(k\cdot x) = \int_0^{k\cdot x} d\phi h(\phi) = \int_0^{k\cdot x} d\phi\left\{h_1f_1(\phi) + h_2f_2(\phi) + h_0\left[f_1^2(\phi) + f_2^2(\phi)\right]\right\}, \tag{9}$$

which implicitely defines $h(\phi)$ with

$$h_0 = -\frac{1}{2}(\mu m_e c)^2 \left(\frac{1}{k\cdot p_{e^-}} + \frac{1}{k\cdot p_{e^+}}\right), \tag{10}$$

$$h_i = \mu m_e c \left(\frac{\varepsilon_i \cdot p_{e^-}}{k\cdot p_{e^-}} - \frac{\varepsilon_i \cdot p_{e^+}}{k\cdot p_{e^+}}\right), \qquad i = 1,2. \tag{11}$$

Moreover, in Eq. (8) we have also

$$\begin{aligned}\mathcal{C}^0(k\cdot x) = {} & g_{00} + (g_{10}+g_{01}) f_1(k\cdot x) \\ & + (g_{20}+g_{02}) f_2(k\cdot x) + g_{11} f_1^2(k\cdot x) \\ & + (g_{12}+g_{21}) f_1(k\cdot x) f_2(k\cdot x) + g_{22} f_2^2(k\cdot x),\end{aligned} \tag{12}$$

with the coefficients $g_{ij}$ $(i,j = 1,2)$ defined as

$$g_{00} = \bar{u}^{(+)}_{\boldsymbol{p}_{e^-}\lambda_{e^-}} \gamma^0 u^{(-)}_{\boldsymbol{p}_{e^+}\lambda_{e^+}}, \tag{13}$$

$$g_{i0} = -\frac{\mu m_e c}{2(k\cdot p_{e^-})} \bar{u}^{(+)}_{\boldsymbol{p}_{e^-}\lambda_{e^-}} \not{\varepsilon}_i \not{k} \gamma^0 u^{(-)}_{\boldsymbol{p}_{e^+}\lambda_{e^+}}, \tag{14}$$

$$g_{0i} = -\frac{\mu m_e c}{2(k\cdot p_{e^+})} \bar{u}^{(+)}_{\boldsymbol{p}_{e^-}\lambda_{e^-}} \gamma^0 \not{\varepsilon}_i \not{k} u^{(-)}_{\boldsymbol{p}_{e^+}\lambda_{e^+}}, \tag{15}$$

$$g_{ij} = \frac{(\mu m_e c)^2}{4(k\cdot p_{e^-})(k\cdot p_{e^+})} \bar{u}^{(+)}_{\boldsymbol{p}_{e^-}\lambda_{e^-}} \not{\varepsilon}_i \not{k} \gamma^0 \not{\varepsilon}_j \not{k} u^{(-)}_{\boldsymbol{p}_{e^+}\lambda_{e^+}}. \tag{16}$$

Let us express the $S$-matrix element (6) in the light-cone variables [31],

$$\begin{aligned}S_{\rm fi} = {} & -iZ\alpha \frac{m_e c^2}{V\sqrt{E_{\boldsymbol{p}_{e^-}} E_{\boldsymbol{p}_{e^+}}}} \int d^4x \, \frac{\mathcal{C}^0(k^0 x^-)}{\sqrt{(\boldsymbol{x}^\perp)^2 + (x^+ - \frac{x^-}{2})^2}} \\ & \times e^{-i(Q^- x^+ + Q^+ x^- - \boldsymbol{Q}^\perp \boldsymbol{x}^\perp) - iH(k^0 x^-)}.\end{aligned} \tag{17}$$

Performing here integrals with respect to $\boldsymbol{x}^\perp$ and $x^+$, we arrive at

$$\begin{aligned}S_{\rm fi} = {} & -iZ\alpha \frac{m_e c^2}{V\sqrt{E_{\boldsymbol{p}_{e^-}} E_{\boldsymbol{p}_{e^+}}}} \frac{4\pi}{(\boldsymbol{Q}^\perp)^2 + (Q^-)^2} \\ & \times \int dx^- \mathcal{C}^0(k^0 x^-) \exp[-iQ^0 x^- - iH(k^0 x^-)].\end{aligned} \tag{18}$$

We note that in the present case both conditions $\boldsymbol{Q}^\perp = \boldsymbol{0}$ and $Q^- = 0$ cannot be simultaneously satisfied, which means that the denominator in the above equation does not vanish.

At this point, let us note that the integral in Eq. (18) has to be transformed, similar to the transformation introduced by Boca and Florescu [26] in the context of Compton scattering. Following the procedure defined in Ref. [31], it can be shown that the replacement should be made,

$$\begin{aligned}& \int dx^- \exp[-iQ^0 x^- - iH(k^0 x^-)] \\ & \to -\frac{k^0}{Q^0} \int dx^- h(k^0 x^-) \exp[-iQ^0 x^- - iH(k^0 x^-)],\end{aligned} \tag{19}$$

which consequently leads to a redefinition of the matrix element $\mathcal{C}^0(k^0 x^-)$ in Eq. (18). Note that the above transformation is justified provided that $Q^0 \neq 0$, which is exactly the case. In the next step, we represent the phase in (18) as

$$Q^0 x^- + H(k^0 x^-) = \bar{Q}^0 x^- + G(k^0 x^-), \tag{20}$$

where a linear and an oscillatory part with respect to $x^-$ have been separated. More specifically, we have

$$\bar{Q} = Q + \big[h_1 \langle f_1\rangle + h_2 \langle f_2\rangle + h_0\big(\langle f_1^2\rangle + \langle f_2^2\rangle\big)\big]k, \tag{21}$$

and

$$\begin{aligned}G(k\cdot x) = {} & \int_0^{k\cdot x} d\phi \big\{h_1(f_1(\phi) - \langle f_1\rangle) + h_2[f_2(\phi) - \langle f_2\rangle] \\ & + h_0\big[f_1^2(\phi) - \langle f_1^2\rangle + f_2^2(\phi) - \langle f_2^2\rangle\big]\big\},\end{aligned} \tag{22}$$

where it is understood that

$$\langle f_i\rangle = \frac{1}{2\pi}\int_0^{2\pi} d\phi f_i(\phi) = \frac{1}{T_{\rm p}}\int_0^{T_{\rm p}} dt f_i(ck^0 t - \boldsymbol{k}\cdot\boldsymbol{r}), \tag{23}$$

for $i = 1,2$, and similarly for $\langle f_i^2\rangle$. When separating linear and periodic parts in Eq. (20), the so-called laser-field-dressed momenta can also be introduced [31,34]

$$\begin{aligned}\bar{p} = {} & p - \beta \mu m_e c \left[\frac{\varepsilon_1\cdot p}{k\cdot p}\langle f_1\rangle + \frac{\varepsilon_2\cdot p}{k\cdot p}\langle f_2\rangle\right]k \\ & + \frac{1}{2}(\mu m_e c)^2 \frac{\langle f_1^2\rangle + \langle f_2^2\rangle}{k\cdot p} k.\end{aligned} \tag{24}$$

Due to the presence of terms which are linear in $\langle f_i\rangle$ $(i = 1,2)$ in Eq. (24), one can anticipate that the electron $(\beta = +1)$ and positron $(\beta = -1)$ response to a finite laser pulse can be very different. This will be investigated later on when analyzing spectra of created pairs.

In the integrand in Eq. (18), we deal now with terms, which can be Fourier decomposed,

$$[f_1(k^0 x^-)]^n [f_2(k^0 x^-)]^m e^{-iG(k^0 x^-)} = \sum_N G_N^{(n,m)} e^{-iNk^0 x^-}, \tag{25}$$

where $n,m = 0,1,2$, and where the case when $n = m = 0$ has been eliminated by the transformation (19). Using the above Fourier expansion, we end up with integrals,

$$\begin{aligned}& \int_0^{2\pi/k^0} dx^- e^{-i(Nk^0 - \bar{p}^0_{e^-} - \bar{p}^0_{e^+})x^-} \\ & = \frac{1 - e^{-2\pi i(Nk^0 - \bar{p}^0_{e^-} - \bar{p}^0_{e^+})/k^0}}{i(Nk^0 - \bar{p}^0_{e^-} - \bar{p}^0_{e^+})}.\end{aligned} \tag{26}$$

Thus, the $S$-matrix amplitude (18) becomes,

$$\begin{aligned}S_{\rm fi} = {} & -\frac{Z\alpha m_e c^2}{V\sqrt{E_{\boldsymbol{p}_{e^-}} E_{\boldsymbol{p}_{e^+}}}} \\ & \times \frac{4\pi}{(\boldsymbol{p}^\perp_{e^-} + \boldsymbol{p}^\perp_{e^+})^2 + (p^0_{e^-} + p^0_{e^+} - \boldsymbol{n}\cdot\boldsymbol{p}_{e^-} - \boldsymbol{n}\cdot\boldsymbol{p}_{e^+})^2} \\ & \times \sum_N \mathcal{C}^0_N \frac{1 - e^{-2\pi i(Nk^0 - \bar{p}^0_{e^-} - \bar{p}^0_{e^+})/k^0}}{Nk^0 - \bar{p}^0_{e^-} - \bar{p}^0_{e^+}},\end{aligned} \tag{27}$$

where the transformed coefficients $\mathcal{C}_N^0$ are defined as

$$\begin{aligned}\mathcal{C}_N^0 = &\left(g_{10}+g_{01}+g_{00}\frac{k^0h_1}{p_{e^-}^0+p_{e^+}^0}\right)G_N^{(1,0)}\\ &+\left(g_{20}+g_{02}+g_{00}\frac{k^0h_2}{p_{e^-}^0+p_{e^+}^0}\right)G_N^{(0,1)}\\ &+\left(g_{11}+g_{00}\frac{k^0h_0}{p_{e^-}^0+p_{e^+}^0}\right)G_N^{(2,0)}\\ &+\left(g_{22}+g_{00}\frac{k^0h_0}{p_{e^-}^0+p_{e^+}^0}\right)G_N^{(0,2)}\\ &+(g_{12}+g_{21})G_N^{(1,1)}.\end{aligned} \tag{28}$$

Let us note that based on Eq. (27), one recovers the appropriate expression for the $S$-matrix amplitude in the monochromatic limit. In the latter case, the summation parameter $N$ has a clear interpretation as a number of laser photons exchanged by the nucleus with the field in order to produce pairs. A similar interpretation is justified for a laser pulse train, which will be discussed in the next section.

Based on Eq. (27), one can define the probability of electron-positron pair creation due to the laser-nucleus interaction,

$$\mathsf{P}^{(\mathrm{p})}=\sum_{\{\lambda\}}\int\frac{Vd^3p_{e^-}}{(2\pi)^3}\frac{Vd^3p_{e^+}}{(2\pi)^3}\,|S_{\mathrm{fi}}|^2. \tag{29}$$

Here, $|S_{\mathrm{fi}}|^2$ describes the respective probability of pair creation between well-defined momentum and spin states of particles. In addition, the integration over the density of final momentum states of electrons $Vd^3p_{e^-}/(2\pi)^3$ and positrons $Vd^3p_{e^+}/(2\pi)^3$ is performed. Finally, the symbol $\sum_{\{\lambda\}}=\sum_{\lambda_{e^-}=\pm}\sum_{\lambda_{e^+}=\pm}$ denotes summation with respect to the final spin degrees of freedom. Having this in mind, we can rewrite the formula defining the probability of pair creation (29) by a single laser pulse,

$$\begin{aligned}\mathsf{P}^{(\mathrm{p})}=&\frac{Z^2\alpha^2m_e^2}{4\pi^4}\sum_{\{\lambda\}}\int dE_{\boldsymbol{p}_{e^-}}dE_{\boldsymbol{p}_{e^+}}d\Omega_{\boldsymbol{p}_{e^-}}d\Omega_{\boldsymbol{p}_{e^+}}\frac{|\boldsymbol{p}_{e^-}||\boldsymbol{p}_{e^+}|}{\left[(\boldsymbol{p}_{e^-}^{\perp}+\boldsymbol{p}_{e^+}^{\perp})^2+(p_{e^-}^0+p_{e^+}^0-\boldsymbol{n}\cdot\boldsymbol{p}_{e^-}-\boldsymbol{n}\cdot\boldsymbol{p}_{e^+})^2\right]^2}\\ &\times\left|\sum_N\mathcal{C}_N^0\,\frac{1-e^{-2\pi i(Nk^0-\bar{p}_{e^-}^0-\bar{p}_{e^+}^0)/k^0}}{Nk^0-\bar{p}_{e^-}^0-\bar{p}_{e^+}^0}\right|^2,\end{aligned} \tag{30}$$

where we used the fact that $d^3p_{e^\pm}=|\boldsymbol{p}_{e^\pm}|p_{e^\pm}^0dp_{e^\pm}^0d\Omega_{\boldsymbol{p}_{e^\pm}}$.

Based on this equation, we can define the differential probability distribution of pair creation by a single laser pulse,

$$\begin{aligned}\frac{d^6\mathsf{P}^{(\mathrm{p})}}{dE_{\boldsymbol{p}_{e^-}}dE_{\boldsymbol{p}_{e^+}}d\Omega_{\boldsymbol{p}_{e^-}}d\Omega_{\boldsymbol{p}_{e^+}}}=&\frac{Z^2\alpha^2m_e^2}{4\pi^4}\sum_{\{\lambda\}}\frac{|\boldsymbol{p}_{e^-}||\boldsymbol{p}_{e^+}|}{\left[(\boldsymbol{p}_{e^-}^{\perp}+\boldsymbol{p}_{e^+}^{\perp})^2+(p_{e^-}^0+p_{e^+}^0-\boldsymbol{n}\cdot\boldsymbol{p}_{e^-}-\boldsymbol{n}\cdot\boldsymbol{p}_{e^+})^2\right]^2}\\ &\times\left|\sum_N\mathcal{C}_N^0\,\frac{1-e^{-2\pi i(Nk^0-\bar{p}_{e^-}^0-\bar{p}_{e^+}^0)/k^0}}{Nk^0-\bar{p}_{e^-}^0-\bar{p}_{e^+}^0}\right|^2,\end{aligned} \tag{31}$$

such that

$$\begin{aligned}\mathsf{P}^{(\mathrm{p})}=&\int dE_{\boldsymbol{p}_{e^-}}dE_{\boldsymbol{p}_{e^+}}d\Omega_{\boldsymbol{p}_{e^-}}d\Omega_{\boldsymbol{p}_{e^+}}\\ &\times\frac{d^6\mathsf{P}^{(\mathrm{p})}}{dE_{\boldsymbol{p}_{e^-}}dE_{\boldsymbol{p}_{e^+}}d\Omega_{\boldsymbol{p}_{e^-}}d\Omega_{\boldsymbol{p}_{e^+}}}.\end{aligned} \tag{32}$$

Let us note that in the sum over $N$ in Eq. (31), the main contribution in the case of a long laser pulse comes from those terms $N$, which are close to $N_{\mathrm{eff}}$, where $N_{\mathrm{eff}}k^0-\bar{p}_{e^-}^0-\bar{p}_{e^+}^0=0$. This means that $N_{\mathrm{eff}}ck^0$ is the energy absorbed from the laser pulse,

$$N_{\mathrm{eff}}=\frac{\bar{p}_{e^-}^0+\bar{p}_{e^+}^0}{k^0}=cT_{\mathrm{p}}\frac{\bar{p}_{e^-}^0+\bar{p}_{e^+}^0}{2\pi}. \tag{33}$$

To have an analogy with the case of a laser pulse train discussed in the next section, we redefine the differential probability of pair creation such that

$$\begin{aligned}&\frac{d^6\mathsf{P}^{(\mathrm{p})}}{dN_{\mathrm{eff}}dE_{\boldsymbol{p}_{e^-}}d\Omega_{\boldsymbol{p}_{e^-}}d\Omega_{\boldsymbol{p}_{e^+}}}\\ &=\left|\frac{dE_{\boldsymbol{p}_{e^+}}}{dN_{\mathrm{eff}}}\right|\frac{d^6\mathsf{P}^{(\mathrm{p})}}{dE_{\boldsymbol{p}_{e^-}}dE_{\boldsymbol{p}_{e^+}}d\Omega_{\boldsymbol{p}_{e^-}}d\Omega_{\boldsymbol{p}_{e^+}}},\end{aligned} \tag{34}$$

where $dE_{\boldsymbol{p}_{e^+}}/dN_{\mathrm{eff}}$ is calculated numerically. We shall refer to the above distribution in Sec. IV when presenting our numerical results.

### B. Laser pulse train

In this section, we present the theory of the nonlinear Bethe-Heitler process, which is induced by a laser pulse train. Within the train, a single laser pulse lasts for time $T_{\mathrm{p}}$, which defines also its fundamental frequency $\omega=2\pi/T_{\mathrm{p}}$. If $\boldsymbol{n}$ determines direction in which the pulse train propagates in space then its four-vector $k$ becomes $k=k^0(1,\boldsymbol{n})$, with $k^0=\omega/c$. We

assume also that the train of pulses is described by the four-vector potential given by Eq. (1), although the condition (2) is not satisfied this time (for more details, see Ref. [31]). Since in the present case, we have that $k \cdot k = 0$ and $k \cdot A(k \cdot x) = 0$ the approach based on the Volkov states introduced in Sec. II is still valid. In fact, all derivations that lead to Eq. (18) are the same for a single laser pulse and for a train of pulses.

Let us go back to Eq. (18). In the current case, there is no need to transform the integral over $x^-$, which means that $\mathcal{C}^0(k^0x^-)$ present there is determined by Eq. (12). We also find that the definitions of $\bar{Q}$ and $G(k^0x^-)$ still hold if we put $\langle f_i \rangle = 0$ $(i = 1,2)$ in Eqs. (21) and (22), respectively. The same applies for the laser-dressed four-momenta of product particles, which means that

$$\bar{p} = p + \frac{1}{2}(\mu m_e c)^2 \frac{\langle f_1^2 \rangle + \langle f_2^2 \rangle}{k \cdot p} k. \tag{35}$$

Having this established, we perform the respective integral in (18) using the following Fourier expansion,

$$\mathcal{C}^0(k^0x^-)\, e^{-iG(k^0x^-)} = \sum_N G_N\, e^{-iNk^0x^-}, \tag{36}$$

where $N$ can be interpreted such that $Nck^0$ is a net energy absorbed from the laser field. As a result, we obtain the final formula for the $S$-matrix amplitude,

$$S_{\mathrm{fi}} = -8i\pi^2 \frac{Z\alpha m_e c^2}{V\sqrt{E_{\boldsymbol{p}_{e^-}} E_{\boldsymbol{p}_{e^+}}}} \times \sum_N \frac{G_N}{(\bar{\boldsymbol{p}}_{e^-} + \bar{\boldsymbol{p}}_{e^+} - N\boldsymbol{k})^2}\, \delta(\bar{p}^0_{e^-} + \bar{p}^0_{e^+} - Nk^0), \tag{37}$$

where the $\delta$ function expresses here the energy conservation law. Let us note that by using this conservation law and the definition (24) one can rewrite the denominator $(\bar{\boldsymbol{p}}_{e^-} + \bar{\boldsymbol{p}}_{e^+} - N\boldsymbol{k})^2$ in exactly the same form as in Eq. (27) using $\boldsymbol{p}^{\perp}_{e^\pm}$, $p^0_{e^\pm}$, and $\boldsymbol{n} \cdot \boldsymbol{p}_{e^\pm}$.

The total probability rate of pair creation induced by a laser pulse train can be defined as

$$W = \sum_{\{\lambda\}} \int \frac{V d^3p_{e^-}}{(2\pi)^3} \frac{V d^3p_{e^+}}{(2\pi)^3} \frac{|S_{\mathrm{fi}}|^2}{T}. \tag{38}$$

Using the prescription that $2\pi[\delta(\bar{p}^0_{e^-} + \bar{p}^0_{e^+} - Nk^0)]^2 \to cT\delta(\bar{p}^0_{e^-} + \bar{p}^0_{e^+} - Nk^0)$ (see, for instance, Ref. [54]), we obtain

$$\frac{|S_{\mathrm{fi}}|^2}{T} = 4(2\pi)^3 \frac{Z^2\alpha^2 m_e^2 c^5}{V^2 E_{\boldsymbol{p}_{e^-}} E_{\boldsymbol{p}_{e^+}}} \times \sum_N \frac{|G_N|^2}{(\bar{\boldsymbol{p}}_{e^-} + \bar{\boldsymbol{p}}_{e^+} - N\boldsymbol{k})^4}\, \delta(\bar{p}^0_{e^-} + \bar{p}^0_{e^+} - Nk^0). \tag{39}$$

Putting the above expression into Eq. (38), we arrive at

$$W = \frac{Z^2\alpha^2 m_e^2 c}{2\pi^3} \sum_N \sum_{\{\lambda\}} \int dE_{\boldsymbol{p}_{e^-}} dE_{\boldsymbol{p}_{e^+}} d\Omega_{\boldsymbol{p}_{e^-}} d\Omega_{\boldsymbol{p}_{e^+}} \times |\boldsymbol{p}_{e^-}||\boldsymbol{p}_{e^+}| \frac{|G_N|^2}{(\bar{\boldsymbol{p}}_{e^-} + \bar{\boldsymbol{p}}_{e^+} - N\boldsymbol{k})^4}\, \delta(\bar{p}^0_{e^-} + \bar{p}^0_{e^+} - Nk^0). \tag{40}$$

With the well-known property,

$$\delta[f(x)] = \sum_\ell \frac{1}{|f'(x^{(\ell)})|} \delta[x - x^{(\ell)}], \tag{41}$$

where $x^{(\ell)}$ is the $\ell$th solution to the equation $f(x) = 0$, we can simplify Eq. (40) such that the total probability rate of pair creation by a laser pulse train becomes

$$W = \frac{Z^2\alpha^2 m_e^2 c^2}{2\pi^3} \sum_N \sum_{\{\lambda\}} \sum_\ell \int dE_{\boldsymbol{p}_{e^-}} d\Omega_{\boldsymbol{p}_{e^-}} d\Omega_{\boldsymbol{p}_{e^+}} \times \frac{|\boldsymbol{p}_{e^-}||\boldsymbol{p}_{e^+}|}{D(p_{e^+})} \frac{|G_N|^2}{(\bar{\boldsymbol{p}}_{e^-} + \bar{\boldsymbol{p}}_{e^+} - N\boldsymbol{k})^4}\bigg|_{E_{\boldsymbol{p}_{e^+}} = E^{(\ell)}_{\boldsymbol{p}_{e^+}}}, \tag{42}$$

with

$$D(p_{e^+}) = \left| 1 + \frac{\bar{p}^0_{e^+} - p^0_{e^+}}{\boldsymbol{p}^2_{e^+}} \left( \frac{k^0}{k \cdot p_{e^+}} (m_e c)^2 - p^0_{e^+} \right) \right|. \tag{43}$$

For details on solving the energy conservation condition with respect to $E_{\boldsymbol{p}_{e^+}}$, see Appendix A. In order to have a meaningful comparison with the case described in Sec. II A we also define another quantity,

$$\mathsf{P}^{(\mathrm{t})} = \frac{2\pi}{ck^0} W, \tag{44}$$

which can be interpreted as a probability of pair creation by an individual laser pulse within the train.

The above equation together with Eq. (42) allow us to define the differential probability of pair creation per one laser pulse from the train. Namely,

$$\frac{d^5\mathsf{P}^{(\mathrm{t})}_N}{dE_{\boldsymbol{p}_{e^-}} d\Omega_{\boldsymbol{p}_{e^-}} d\Omega_{\boldsymbol{p}_{e^+}}} = \frac{(Z\alpha m_e c)^2}{\pi^2 ck^0} \sum_{\{\lambda\}} \sum_\ell \frac{|\boldsymbol{p}_{e^-}||\boldsymbol{p}_{e^+}|}{D(p_{e^+})} \times \frac{|G_N|^2}{(\bar{\boldsymbol{p}}_{e^-} + \bar{\boldsymbol{p}}_{e^+} - N\boldsymbol{k})^4}\bigg|_{E_{\boldsymbol{p}_{e^+}} = E^{(\ell)}_{\boldsymbol{p}_{e^+}}}, \tag{45}$$

which symbolically can be denoted as

$$\frac{d^5\mathsf{P}^{(\mathrm{t})}_N}{dE_{\boldsymbol{p}_{e^-}} d\Omega_{\boldsymbol{p}_{e^-}} d\Omega_{\boldsymbol{p}_{e^+}}} = \frac{d^6\mathsf{P}^{(\mathrm{t})}}{dN dE_{\boldsymbol{p}_{e^-}} d\Omega_{\boldsymbol{p}_{e^-}} d\Omega_{\boldsymbol{p}_{e^+}}}. \tag{46}$$

This quantity will be calculated and compared with the respective differential distribution of created particles by an isolated laser pulse in Sec. IV.

## III. SHAPE FUNCTIONS

Consider a linearly polarized laser pulse, which propagates in the $z$ direction ($\boldsymbol{n} = \boldsymbol{e}_z$), with a polarization vector along the $x$ axis ($\boldsymbol{\varepsilon}_1 = \boldsymbol{e}_x$). Here, $f_2(\phi) = 0$ and $f_1(\phi) = Bf(\phi)$ where the meaning of the constant $B$ will be explained following Eq. (53). Let us assume that the shape function $f'(\phi)$ has the following Fourier expansion,

$$f'(\phi) = \sum_{N=-N_0}^{N=N_0} f'_N e^{-iN\phi}, \tag{47}$$

with a vanishing zero Fourier component $f'_0 = 0$. In order to keep this function real we require that $f'_{-N} = [f'_N]^*$. The

four-vector potential shape function is obtained according to Eq. (B6). For a single laser pulse,

$$f(\phi) = f_0 - \sum_{N=-N_0}^{N=N_0} \frac{f'_N}{iN} e^{-iN\phi}, \tag{48}$$

which means that there is a zero Fourier component but it is chosen such that $f(0) = f(2\pi) = 0$. Hence,

$$f_0 = \sum_{N=-N_0}^{N=N_0} \frac{f'_N}{iN}. \tag{49}$$

As indicated by Eq. (2), the shape function $f(\phi)$ for an individual laser pulse vanishes for $\phi < 0$ and $\phi > 2\pi$. On the other hand, for an infinite sequence of pulses,

$$f_{\text{train}}(\phi) = - \sum_{N=-N_0}^{N=N_0} \frac{f'_N}{iN} e^{-iN\phi}, \tag{50}$$

where the zero Fourier component can be removed using the gauge transformation. In fact, this is necessary if we want to keep the same definition of field-free asymptotic momenta of charged particles, which enter the Volkov solutions [Eqs. (4) and (5)] as in the case of a finite laser pulse. In other words, $f_{\text{train}}(\phi)$ is periodic in $\phi$ and hence, $\langle f_{\text{train}} \rangle = 0$.

We use this scheme for a particular choice of the shape function $f'(\phi)$ defining the electric and magnetic field components. Namely, we choose

$$f'(\phi) = -N_f \sin^2\left(\frac{\phi}{2}\right) \sin(N_{\text{osc}}\phi + \chi), \tag{51}$$

where $\phi = k \cdot x$ changes as $0 \leqslant \phi \leqslant 2\pi$, $N_{\text{osc}}$ defines the number of field oscillations within a pulse, whereas $\chi$ is the carrier-envelope phase (CEP). The normalization constant $N_f$ is chosen such that (Appendix B)

$$\frac{1}{2\pi} \int_0^{2\pi} d\phi [f'(\phi)]^2 = \frac{1}{2}. \tag{52}$$

Next, we introduce the four-vector potential

$$A(k \cdot x) = A_0 B \varepsilon f(k \cdot x), \tag{53}$$

where $\varepsilon = (0, \boldsymbol{e}_x)$, whereas $A_0$ and $B$ are constants chosen such that the mean intensity carried out by the laser pulse does not depend on the pulse duration (see Appendix B). If we define,

$$\mu = \frac{|eA_0|}{m_e c}, \tag{54}$$

then the mean intensity of the electromagnetic radiation in the pulse becomes

$$I = \frac{\mu^2}{8\pi\alpha} B^2 k_0^2 (m_e c^2)^2, \tag{55}$$

which does not depend on $N_{\text{osc}}$ if only $B = N_{\text{osc}}$. Because $N_{\text{osc}} k_0 = \omega_{\text{L}}/c$, where $\omega_{\text{L}}$ is the central frequency of the laser field, we find that

$$I = \frac{\mu^2 \omega_{\text{L}}^2 (m_e c)^2}{8\pi\alpha}. \tag{56}$$

This can be conveniently replaced by the following scaling formula,

$$I = 2.3 \times 10^{29} \mu^2 \omega_{\text{L}}^2, \tag{57}$$

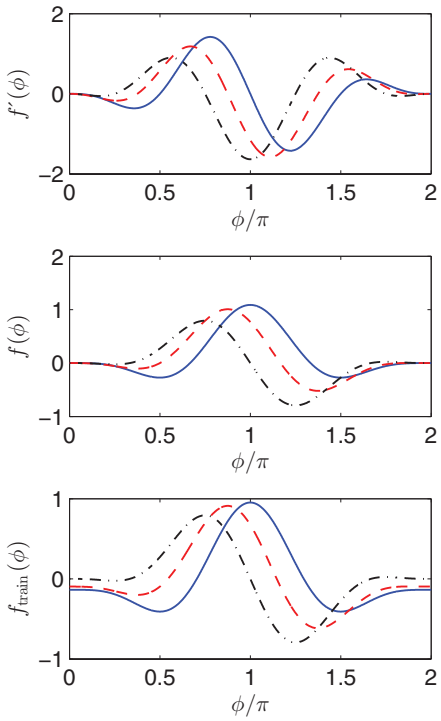


FIG. 1. (Color online) Shape functions for a two-cycle laser pulse ($N_{\text{osc}} = 2$) and different carrier-envelope phases: $\chi = 0$ (solid blue), $\chi = 0.25\pi$ (dashed red), and $\chi = 0.5\pi$ (dash-dotted black). While the top panel shows the shape function for the electric and magnetic field components [Eq. (51)], $f'(\phi)$, in the middle panel the shape function for the vector potential is drawn, $f(\phi)$. In the bottom panel, we plot the shape function for a single pulse within a train, $f_{\text{train}}(\phi)$. Both $f(\phi)$ and $f_{\text{train}}(\phi)$ are calculated based on Eq. (51) (for details, see Sec. III).

where $I$ is expressed in W/cm$^2$, whereas $\omega_{\text{L}}$ is in units of the electron rest energy $m_e c^2$. From now on, we keep the current definition of the parameter $\mu$, which corresponds to a rescaled peak value of the vector potential. By doing so, we compare the pair creation at a fixed averaged intensity of the laser field in the pulse, even though its duration is changed. In order to define a shape function for a train of pulses we repeat $f(\phi)$ [Eq. (51)] for all times, with the zero Fourier component being removed by an appropriate gauge transformation.

Figure 1 illustrates the shape functions $f'(\phi), f(\phi)$, and $f_{\text{train}}(\phi)$ of our choice [Eq. (51) and the following discussion] for different values of the carrier envelope phase. Specifically, we plot these functions for $\chi = 0$ (solid blue line), $\chi = 0.25\pi$ (dashed red line), and $\chi = 0.5\pi$ (dash-dotted black line). Figure 1 corresponds to a very short laser pulse that includes only two oscillations of the electromagnetic field ($N_{\text{osc}} = 2$). One recognizes here that a temporal structure of both the vector potential and the electric (magnetic) field component is very sensitive to a change of the carrier-envelope phase $\chi$. It follows from this figure that $\langle f \rangle$ defining the finite laser pulse can dramatically change with $\chi$. For much longer pulses, this is not the case since $\langle f \rangle$ almost vanishes. The latter is also true for an infinite sequence of identical pulses.

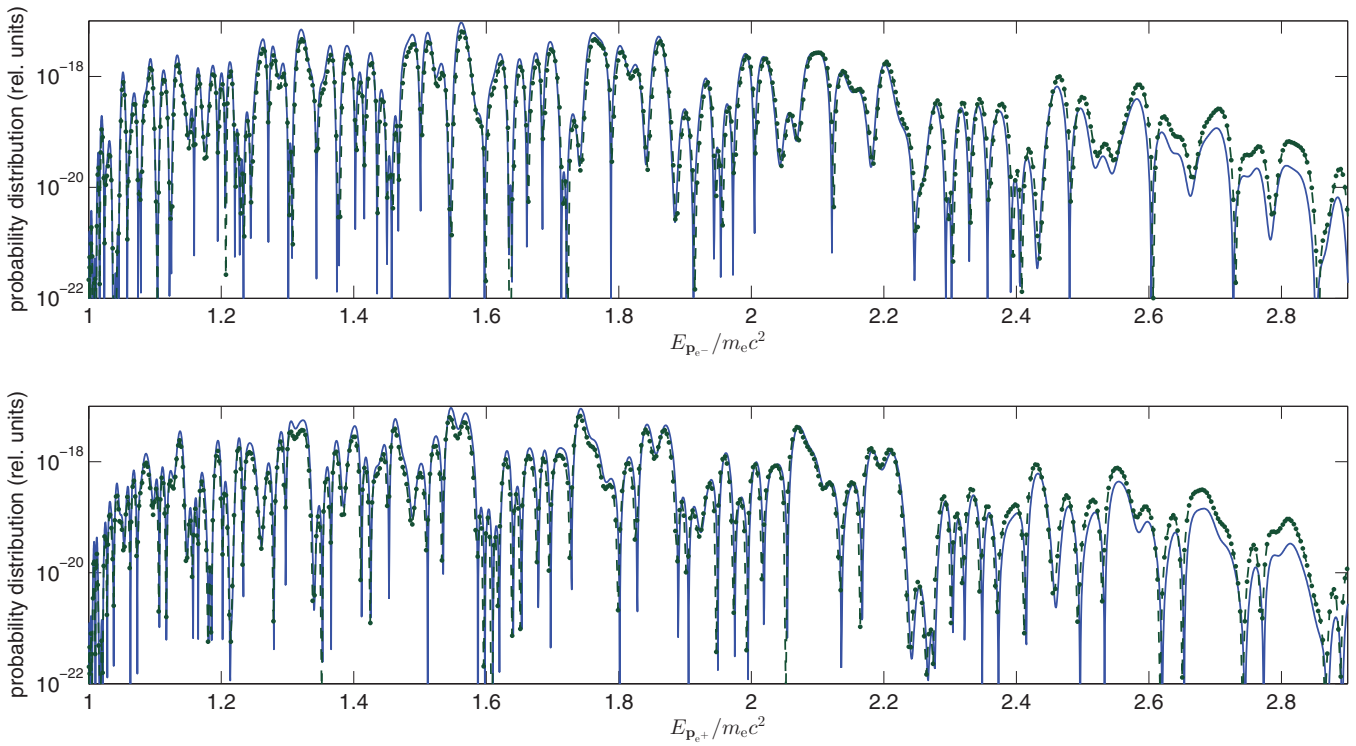


FIG. 2. (Color online) Probability distributions of pair creation by a single laser pulse (blue solid line) and by an individual laser pulse from the train of pulses (green dots) for the laser field parameters: $\mu = 1$, $\omega_L = 0.1\, m_e c^2$, $\chi = 0$, and $N_{osc} = 32$ [Eqs. (34) and (46), respectively]. In the upper row, we present the results for the case when the positron momentum as measured at the detector is fixed such that $|\boldsymbol{p}_{e^+}| = m_e c$, $\varphi_{e^+} = \pi$, and $\theta_{e^+} = 0.7\pi$. In addition, the direction of electron detection is fixed: $\varphi_{e^-} = 0$ and $\theta_{e^-} = 0.8\pi$. In the lower row, the situation is reversed, meaning that this time $|\boldsymbol{p}_{e^-}| = m_e c$, $\varphi_{e^-} = \pi$, $\theta_{e^-} = 0.7\pi$, $\varphi_{e^+} = 0$, and $\theta_{e^+} = 0.8\pi$.

## IV. SPECTRA OF CREATED PARTICLES: SINGLE PULSE VERSUS PULSE TRAIN

In this section, numerical results for probability spectra of created particles in collisions of a proton (treated as an infinitely heavy particle) with an incident laser beam are presented and discussed. For the incident laser field, we choose either an isolated laser pulse or an infinite sequence of such pulses propagating in the $z$ direction and linearly polarized in the $x$ direction, with shape functions introduced in Sec. III. As we have discussed there, we are going to compare the pair creation processes induced by laser pulses of a fixed mean laser-field intensity but for different pulse durations (for details, see Sec. III and Appendix B). Note that the results presented in this and in the following section always refer to the proton frame of reference.

In Fig. 2, we demonstrate probability distributions of Bethe-Heitler process for the case when the driving laser field is either a single pulse (blue solid line) [Eq. (34)] or a sequence of individual pulses (green dots) [Eq. (46)]. In both cases, we keep the same parameters such that the central frequency of the laser field is $\omega_L = 0.1 m_e c^2$, the parameter $\mu = 1$, $\chi = 0$, whereas $N_{osc} = 32$. The top panel illustrates the dependence of differential probability distributions of pair creation on the electron energy $E_{\boldsymbol{p}_{e^-}}$ (measured in units of $m_e c^2$). The presented results are for the case when the electron is detected with the azimuthal and polar angles $\varphi_{e^-} = 0$ and $\theta_{e^-} = 0.8\pi$, respectively. At the same time, its accompanying positron is measured with the momentum such that $|\boldsymbol{p}_{e^+}| = m_e c$, $\varphi_{e^+} = \pi$, and $\theta_{e^+} = 0.7\pi$. The situation is reversed for the bottom panel. Namely, the differential probability distributions are shown there as a function of the positron energy $E_{\boldsymbol{p}_{e^+}}$ (in units of $m_e c^2$) when the positron momentum direction is specified such that $\varphi_{e^+} = 0$ and $\theta_{e^+} = 0.8\pi$. In this case, we have chosen $|\boldsymbol{p}_{e^-}| = m_e c$, $\varphi_{e^-} = \pi$, and $\theta_{e^-} = 0.7\pi$. The choice of these angles has been made to some extent arbitrarily, but deliberately such that the electron and the positron are emitted asymmetrically.

One can conclude from Fig. 2 that there is a good overall agreement between the results for a single laser pulse and for a train of pulses. Note that the spectra presented in Fig. 2 correspond to large numbers $N$ (in the case of a pulse train) and $N_{eff}$ (in the case of a single pulse), which are between 950 and 1600. While for smaller $N$ and $N_{eff}$, corresponding to production of low-energy electrons and positrons, the respective spectra are less sensitive to the actual structure of the driving laser field, with increasing $N$ and $N_{eff}$ (and, hence, also with increasing the energy of produced particles) this sensitivity becomes more evident. In particular, the agreement between the respective spectra might seem not as good as for the nonlinear Compton scattering considered in Ref. [31]. The possible explanation being that there is a nonzero threshold for the pair creation process, which makes the process more sensitive to even a small modification of the driving laser field as compared to the Compton scattering. This would suggest also that the actual temporal structure of the electromagnetic radiation is particularly important in the

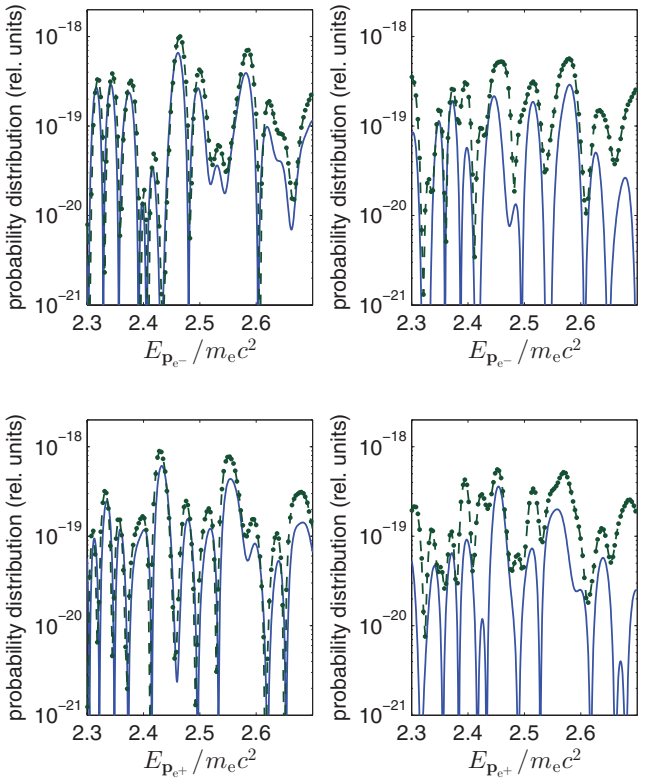


FIG. 3. (Color online) The same as in Fig. 2 but zoomed into the more narrow energy range. Whereas the results shown in the left column are for $\chi = 0$, the results in the right column are for $\chi = 0.4\pi$.

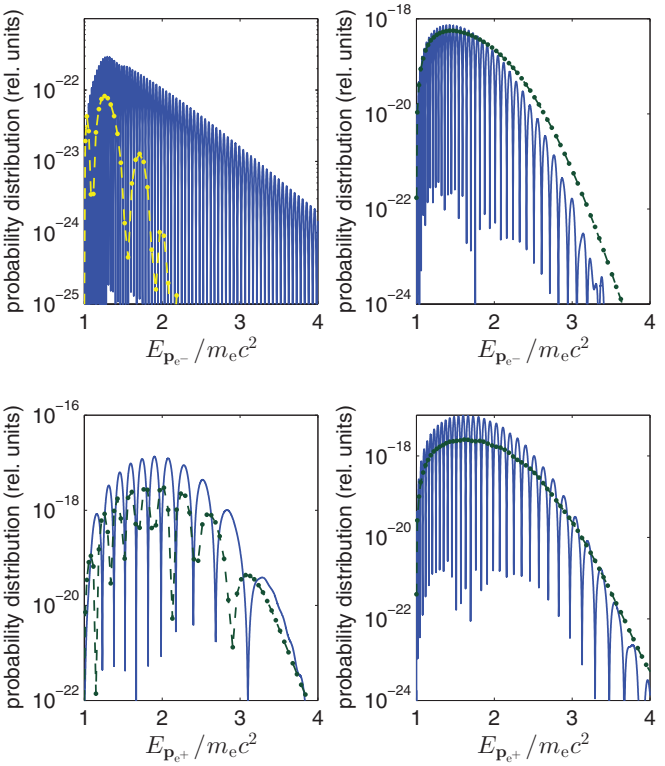


FIG. 4. (Color online) The same as in Fig. 3 but for a much shorter laser pulse, with $N_{\mathrm{osc}} = 2$. In the upper left panel, we use yellow dots instead of green dots for visual purpose.

context of laser-induced pair creation. At the same time, one sees that the spectra are asymmetric with respect to interchange of an electron and a positron. This asymmetry will be even more pronounced for shorter driving laser pulses.

In Fig. 3 we show the same as in Fig. 2 but over a narrow range of the electron and positron energies. Specifically, the left column is for exactly the same parameters as in Fig. 2 while the right column is for a different carrier-envelope phase, $\chi = 0.4\pi$. One has to realize that the agreement between the spectral distributions for a single pulse and a pulse train looks worse only on the scale of the figure. What is important to note here is a change of the distributions with changing the CEP. This is even more pronounced for a two-cycle driving pulse, as shown in Fig. 4.

In Fig. 4, we present the same energy distributions as in Fig. 3 but for the case that only two oscillations of an electromagnetic radiation are contained in the pulse ($N_{\mathrm{osc}} = 2$). We see from this figure that there is not even qualitative agreement between the situation when an incident laser field is a single pulse or a sequence of pulses, which happens even for low-energy electrons (positrons). In particular, a very rich oscillatory structure of the energy spectra present for an individual pulse is washed out for a laser pulses train. Also, as mentioned before, the spectra of produced electrons and positrons can in principle be very different, which for the current choice of the normalized pulse shape is particularly clear when comparing panels corresponding to $\chi = 0$ (i.e., in the left column). This illustrates the fact that the electron and positron responses to a few-cycle laser pulse are very different, due to a different field-dressing of particles and antiparticles (see Sec. II A). In this context one should understand that, in comparison with the monochromatic case where the spectra of electrons and positrons are identical, the finite laser pulse leads to redistribution of the particles. In particular, in Fig. 4 (left column), the amount of electrons is by four orders larger than the amount of positrons. However, the total amount of emitted electrons and positrons must be the same, so the positrons must be emitted into some other angular regions.

It follows from Fig. 1 that the shape functions characterizing the laser field for $\chi = \pi/2$ are symmetric with respect to the change of polarization direction, $\boldsymbol{\varepsilon} \to -\boldsymbol{\varepsilon}$, or, in other words, that $\langle f \rangle = \langle f' \rangle = \langle f_{\mathrm{train}} \rangle = 0$. We expect therefore that the respective energy distributions for an electron and for a positron should be the same, regardless of the incident pulse duration. We have checked this numerically for parameters of Figs. 3 and 4. Indeed, for the carrier envelope phase $\pi/2$ the plots are identical when we interchange an electron with a positron. For this reason, we do not present here the respective results. This also explains why for $\chi = 0.4\pi$, the electron and positron energy spectra presented in the right column of Fig. 4 are quite similar.

All figures discussed so far relate to the nonperturbative regime of laser-induced pair creation such that $\mu = 1$ and $\omega_{\mathrm{L}} = 0.1 m_e c^2$. The question arises: Is the same behavior of probability distributions of product particles observed also in other regimes of laser-matter interaction? To answer this question, we performed calculations for other values of the field parameters; while we observed a reasonable agreement

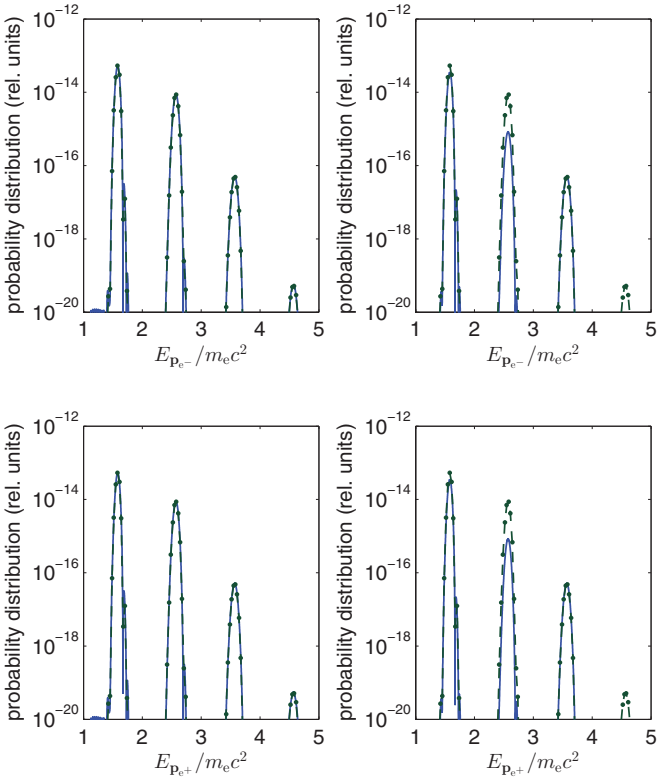


FIG. 5. (Color online) The same as in Fig. 3 but for the laser field parameters: $\mu = 0.1$, $\omega_L = m_e c^2$, and $N_{osc} = 32$.

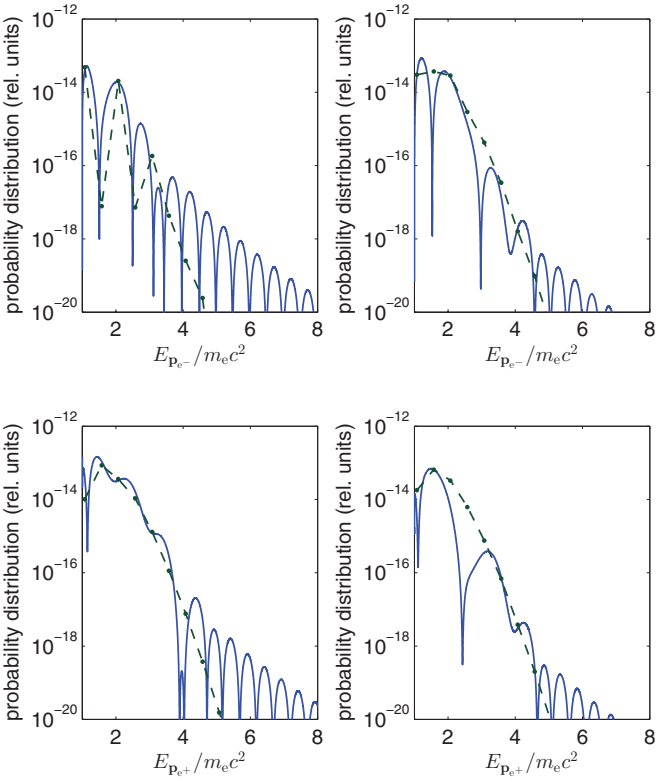


FIG. 6. (Color online) The same as in Fig. 5 but for $N_{osc} = 2$.

between the results for a single pulse and a pulse train when $N_{osc} = 32$, this agreement substantially decreased for $N_{osc} = 2$. Specifically, in Figs. 5 and 6, we present the energy spectra for $\mu = 0.1$ and $\omega_L = m_e c^2$, which correspond to a perturbative regime of laser-induced pair creation. Even though the presented spectra show the exactly same general tendency one can argue, however, that in the perturbative regime the agreement between the results for a pulse and a pulse train is still better than for stronger fields.

In closing this section, we compare the probability distributions of pair creation by a train of laser pulses and by a monochromatic plane wave. The latter can be treated as a train of pulses with a constant envelope in Eq. (51). In other words, in both cases we refer to the distribution defined by Eq. (46). The respective results are presented in Fig. 7. While in the left panel of Fig. 7 we show the results for pair creation induced by a train of pulses, in the right panel we show the corresponding results for a monochromatic plane wave, each of them containing 32 cycles of the laser field within a segment of the envelope. For an illustration, we have chosen the laser field characterized by the following parameters: $\mu = 1$, $\omega_L = 0.1 m_e c^2$, and $\chi = 0$. The other parameters are $|\boldsymbol{p}_{e^-}| = m_e c$, $\varphi_{e^-} = \pi$, $\theta_{e^-} = 0.7\pi$, $\varphi_{e^+} = 0$, and $\theta_{e^+} = 0.8\pi$. The spectra are plotted as a function of the number of laser photons $N$ absorbed from the laser field (in units of $N_{osc}$). It means that the spectra are composed of discrete points, even though in the left panel we have connected these points by straight lines for the visual purpose. In the right panel, on the other hand we keep these points separated (and denote them as stars). Note that the results for a monochromatic plane wave are by more than four orders of magnitude smaller than the corresponding results for a train of pulses. This happens despite the fact that the mean intensity of the laser field contained in the sequence of $N_{osc}$ field cycles is the same in both cases. The point being that despite the same averaged intensity carried out by a monochromatic plane wave or by a train of pulses, the maximum intensity determined by $N_f^2$ [see, Eq. (51)] is almost three times smaller for a monochromatic plane wave.

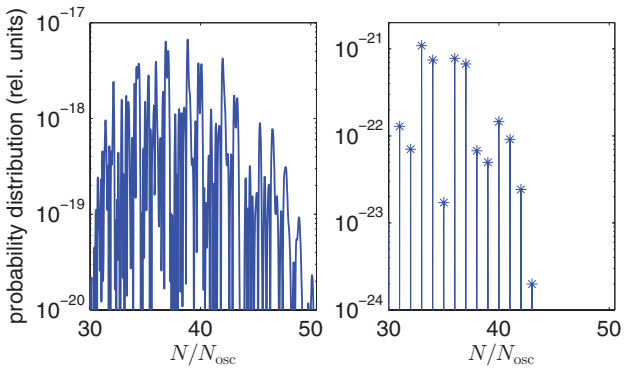


FIG. 7. (Color online) Probability distributions of pair creation as a function of the photon number $N$ absorbed either from a train of pulses (left panel) and from a monochromatic plane wave (right panel), each containing 32 field oscillations ($N_{osc} = 32$). The results are for $\mu = 1$, $\omega_L = 0.1 m_e c^2$, and $\chi = 0$. In addition, we have chosen $|\boldsymbol{p}_{e^-}| = m_e c$, $\varphi_{e^-} = \pi$, $\theta_{e^-} = 0.7\pi$, $\varphi_{e^+} = 0$, and $\theta_{e^+} = 0.8\pi$. The results in the right panel, represented in a stem plot, are multiples of $N_{osc}$. The results in the left panel are also points corresponding to integer $N$, however for visual purposes they have been connected by vertical lines.

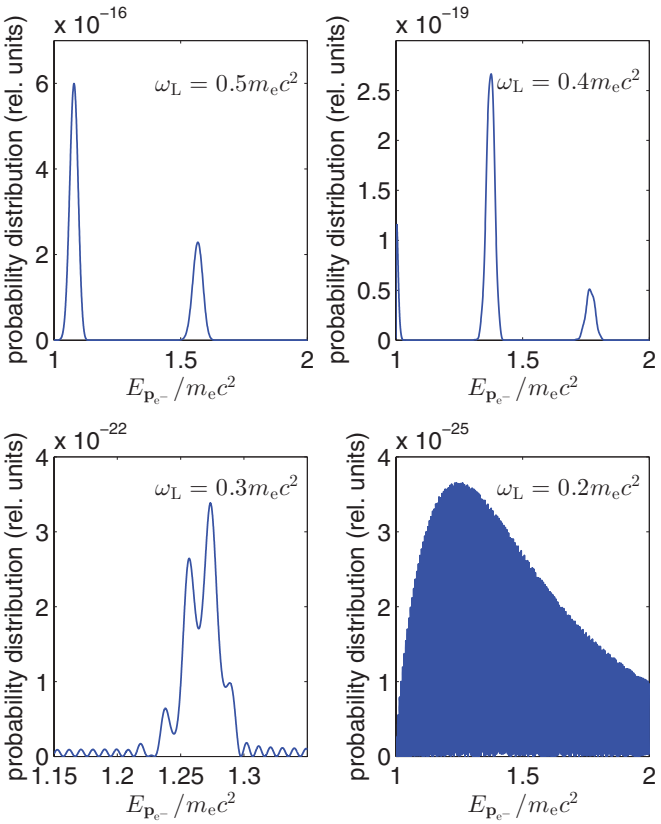


FIG. 8. (Color online) The electron spectra for $\mu = 0.1$ but for different values of $\omega_{\mathrm{L}}$, as indicated in each panel. The results are for the 32-cycle pulse with the CEP equal to 0. The accompanying positron is detected with asymptotic momentum characterized by $|\boldsymbol{p}_{e^+}| = m_e c$, $\varphi_{e^+} = \pi$, $\theta_{e^+} = 0.7\pi$, while the electron direction is specified by $\varphi_{e^-} = 0$ and $\theta_{e^-} = 0.8\pi$.

While it makes sense to compare the electron (positron) spectra for a train of pulses and for a single laser pulse, both with exactly same shape function given by Eq. (51), a similar comparison with a monochromatic plane wave is not that meaningful. We suspect therefore that in order to have a reasonable correspondence to the monochromatic plane wave approximation one should consider a different pulse shape, with the envelope that is constant for mostly all times. This is beyond the scope of the present paper, but the respective analysis will be presented in due course.

## V. PAIR CREATION BY A SINGLE PULSE: IMPACT OF PULSE LENGTH AND FREQUENCY

In Fig. 8, we show the electron energy distributions in the Bethe-Heitler process induced by a finite laser pulse such that $\mu = 0.1$ and for different values of the central frequency $\omega_{\mathrm{L}}$, as indicated in each panel. The remaining parameters of the laser pulse are $N_{\mathrm{osc}} = 32$ and $\chi = 0$, whereas the kinematic parameters of the accompanying positron are $|\boldsymbol{p}_{e^+}| = m_e c$, $\varphi_{e^+} = \pi$, and $\theta_{e^+} = 0.7\pi$. For $\omega_{\mathrm{L}} = 0.5 m_e c^2$, one can clearly see typical multiphoton peaks separated by roughly $\omega_{\mathrm{L}}$ and decreasing in magnitude for higher-order processes. If we decrease the frequency $\omega_{\mathrm{L}}$ to $0.4 m_e c^2$, the first multiphoton peak appears just below the threshold. For still smaller frequency,

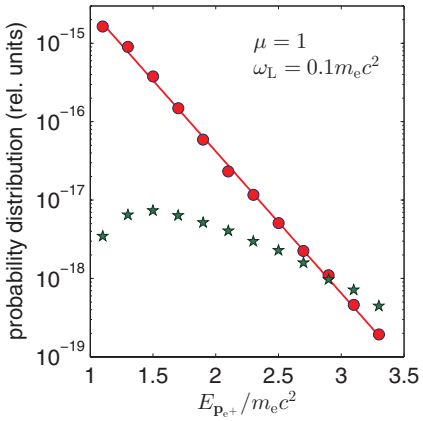


FIG. 9. (Color online) The probability distribution of created positrons as a function of their energy for a 32-cycle (red circles) and a two-cycle (green pentagrams) driving laser pulses. For a 32-cycle pulse, the solid red line represents the fit of the function $P_0 \exp[-(E_{\boldsymbol{p}_{e^+}} - m_e c^2)/E_0]$ to the calculated points, with $P_0 = 2.7 \times 10^{-15}$ (in relativistic units) and $E_0 = 0.24 m_e c^2$. For a two-cycle pulse, the similar fit is less accurate as the respective distribution is not a monotonically decreasing function, at least for the chosen normalization of the pulse. The results are for the laser field parameters such that $\mu = 1$ and $\omega_{\mathrm{L}} = 0.1 m_e c^2$, as indicated in the figure.

$\omega_{\mathrm{L}} = 0.3 m_e c^2$, only the first dominant peak survives, which, in addition, splits into subpeaks. Note that the magnitude of this dominant peak has decreased in magnitude such that the tiny background oscillations becomes visible on the scale of the figure. The frequency of these regular background oscillations corresponds to the fundamental frequency of the laser field, $\omega$, which in the present case is slightly less than $0.01 m_e c^2$. With still decreasing $\omega_{\mathrm{L}}$, the dominant peak decreases and eventually, for $\omega_{\mathrm{L}} = 0.2 m_e c^2$, it cannot be distinguished any longer from the background oscillations. It is interesting to note that the results presented in Fig. 8 for central frequencies ranging from $0.5 m_e c^2$ down to $0.2 m_e c^2$ resemble the transition from the multiphoton regime to the tunneling (or quasistatic) regime of pair creation. While for the high frequencies we observe very well separated multiphoton peaks, the spectrum turns into a smooth and very broad distribution for the lowest frequency.

In Fig. 9, we present the positron probability distributions for a 32-cycle (red circles) and a two-cycle (green pentagrams) driving laser pulses for which $\omega_{\mathrm{L}} = 0.1 m_e c^2$ and $\mu = 1$. The results were obtained by performing the five-dimensional integral out of the six-dimensional integral in Eq. (32), i.e., by leaving out the integration with respect to the positron energy, $E_{\boldsymbol{p}_{e^+}}$. The remaining five-dimensional integral was calculated using the Monte Carlo method [11] with $2 \times 10^6$ sample points in each run. While the integration over the electron and positron momentum directions was performed over the whole solid angle, the upper limit for the integral over the electron energy was set to $10 m_e c^2$. This particular choice of the energy cutoff is consistent with the obtained results in the sense that for the positron energy bigger than $3 m_e c^2$, the results are already by an order of magnitude smaller than the respective maximum. Note that in the current case

the results carry the error less than 10%. In order to assure that the Monte Carlo method is stable, we also performed calculations for other parameters; for instance, we increased number of sample points to $10^7$ and limited the integration over $E_{\boldsymbol{p}_{e^-}}$ to $5m_ec^2$. In this case, the Monte Carlo results carried the error less than 10% for bigger positron energies and less than 1% for smaller positron energies. The difference between the calculated spectra and the results of Fig. 9 turned out to be hardly noticeable. Finally, we calculated the exactly same probability distributions as in Fig. 9 but as a function of the electron energy. The corresponding distribution, integrated over the positron momentum and the electron detection angles, turned out to be identical as the one shown in Fig. 9.

The results for the 32-cycle pulse presented in Fig. 9, seem to fit very well with the function $P_0 \exp\left[-(E_{\boldsymbol{p}_{e^+}} - m_ec^2)/E_0\right]$ for the estimated parameters $P_0 = 2.7 \times 10^{-15}$ (in relativistic units) and $E_0 = 0.24m_ec^2$; the latter represented in Fig. 9 by the solid line. For the two-cycle laser pulse, the similar fit is not justified. In this case, the probability distribution is not a monotonically decreasing function of the positron energy; in fact, the distribution increases monotonically for small values of the positron energy and, only after reaching the maximum, it starts to decrease. It also follows from Fig. 9 that the probability distribution of created positrons is much smaller for short laser pulses than for long laser pulses in the regime where the low-energy positrons are created. This holds, however, for the chosen normalization of the driving laser pulse, i.e., when the peak vector potential scales with $N_{\mathrm{osc}}$ [see Eq. (53) and the following discussion].

## VI. CONCLUSION

In this paper, the Bethe-Heitler scenario of $e^-e^+$ pair creation by a finite laser pulse was investigated. Specifically, we considered the pair creation in a collision of a laser pulse with a proton, which was treated as an infinitely massive particle. In other words, we neglected the proton recoil while we studied the purely pulse-related effects on the pair creation process.

The spectra of positrons and electrons for a single laser pulse have been compared with the corresponding spectra for an infinite sequence of such pulses. We found a very good agreement between the particles spectra in these two cases if the driving pulse is sufficiently long. However, as illustrated by various examples, there are dramatic qualitative and quantitative differences between the created particles spectra in the aforementioned cases if the driving pulse is short. The reason being that the dynamics of the Bethe-Heitler process (and other laser-induced processes as well; see, for instance, Refs. [31,34]) depends on the actual temporal behavior of the driving field. This has been also demonstrated by looking at the carrier-envelope phase effects on the positron and electron spectra.

In closing, we note that the pair creation is a threshold-related effect and therefore it is very sensitive to the features of a driving laser field, which happens also for above-threshold ionization of atoms and negative ions [55,56]. In the current work we observed, for instance, that the probability distributions of created pairs for a pulse train with a sine-squared envelope disagree with respective results for a pulse train with a constant envelope. In this context, it would be further interesting to closely analyze the shape effects on the Bethe-Heitler process when driven by a finite pulse. This is a topic for future research.

## ACKNOWLEDGMENTS

This work is supported by the Polish National Science Center (NCN) under Grant No. 2011/01/B/ST2/00381. K.K. gratefully acknowledges the hospitality of the Max Planck Institut für Kernphysik, Heidelberg, Germany.

## APPENDIX A: SOLVING THE ENERGY CONSERVATION CONDITION

Let us analyze solutions of the following conservation condition,

$$\bar{p}^0 + \kappa = 0, \tag{A1}$$

where $\bar{p}$ is an unknown four-vector such that

$$\bar{p} = p + \zeta \frac{n}{n \cdot p}. \tag{A2}$$

In accordance with Eq. (35), $\zeta = \frac{1}{2}(\mu m_ec)^2(\langle f_1^2\rangle + \langle f_2^2\rangle)$. Moreover, $n = (1,\boldsymbol{n})$ and we assume that the direction of the vector $\boldsymbol{p}$ is known; we further denote it as $\boldsymbol{n}_p$. For now, $\kappa$ is a known constant. Note also that $\bar{p} \cdot \bar{p} = (m_ec)^2 + 2\zeta$, which follows from Eq. (A2).

Having this in mind, Eq. (A1) can be rewritten as,

$$(p^0 + \kappa)(n \cdot p) + \zeta = 0, \tag{A3}$$

where one should remember that $|\boldsymbol{p}| = \sqrt{(p^0)^2 - (m_ec)^2}$. Substituting this relation into the last equation, we derive the following fourth-order equation to be satisfied by $p^0$,

$$\begin{aligned}&[1 - (\boldsymbol{n} \cdot \boldsymbol{n}_p)^2](p^0)^4 + 2\kappa[1 - (\boldsymbol{n} \cdot \boldsymbol{n}_p)^2](p^0)^3 \\ &\quad + \{2\zeta + (m_ec)^2(\boldsymbol{n} \cdot \boldsymbol{n}_p)^2 + \kappa^2[1 - (\boldsymbol{n} \cdot \boldsymbol{n}_p)^2]\}(p^0)^2 \\ &\quad + 2\kappa[\zeta + (m_ec)^2(\boldsymbol{n} \cdot \boldsymbol{n}_p)^2]p^0 \\ &\quad + \kappa^2(m_ec)^2(\boldsymbol{n} \cdot \boldsymbol{n}_p)^2 + \zeta^2 = 0.\end{aligned} \tag{A4}$$

Solving this equation for the fixed direction $\boldsymbol{n}_p$, we are able to determine the energy $E_{\boldsymbol{p}} = cp^0$ and hence also the momentum $\boldsymbol{p}$. Among all four solutions of the above equation, $p^{0(\ell)}$ where $\ell = 1,2,3,4$, we choose only those which are real and greater than $m_ec$. In particular, for the analysis presented in this paper we have

$$\bar{p}^0 = \bar{p}^0_{e^+}, \quad \kappa = \bar{p}^0_{e^-} - Nk^0, \tag{A5}$$

in the energy conservation law (40).

## APPENDIX B: LASER PULSE ENERGY

For a laser pulse, the electric and magnetic components of the field are

$$\begin{aligned}\boldsymbol{\mathcal{E}}(k \cdot x) &= -ck_0A_0[\boldsymbol{\varepsilon}_1 f_1'(k \cdot x) + \boldsymbol{\varepsilon}_2 f_2'(k \cdot x)], \\ \boldsymbol{\mathcal{B}}(k \cdot x) &= -k_0A_0[\boldsymbol{n} \times \boldsymbol{\varepsilon}_1 f_1'(k \cdot x) + \boldsymbol{n} \times \boldsymbol{\varepsilon}_2 f_2'(k \cdot x)],\end{aligned} \tag{B1}$$

where $\boldsymbol{n}$ defines the propagation direction of the pulse, whereas $\boldsymbol{\varepsilon}_i$ are real polarization vectors. Here, *prime* means a derivative

with respect to $k \cdot x$. If the laser pulse duration is $T_{\rm p}$, the wave four-vector is

$$k = k_0(1,\boldsymbol{n}), \quad k_0 = 2\pi/(cT_{\rm p}). \tag{B2}$$

Since the electromagnetic field generated by lasers has to fulfill the following condition [46]

$$\int_{-\infty}^{\infty} \boldsymbol{\mathcal{E}}(ck^0 t - \boldsymbol{k}\cdot\boldsymbol{r})dt = 0, \tag{B3}$$

the shape functions $f_i'(\phi)$, which vanish for $\phi < 0$ and $\phi > 2\pi$, are such that

$$\int_0^{2\pi} d\phi f_i'(\phi) = 0. \tag{B4}$$

Hence, the four-vector potential describing the pulse has the form

$$A(x) = A_0[\varepsilon_1 f_1(k\cdot x) + \varepsilon_2 f_2(k\cdot x)], \tag{B5}$$

where the respective shape functions defined as

$$f_i(k\cdot x) = \int_0^{k\cdot x} d\phi f_i'(\phi), \tag{B6}$$

are zero when $\phi < 0$ and $\phi > 2\pi$.

The Poynting vector $\boldsymbol{S}$ defining the power flux density carried out by the electromagnetic radiation [Eq. (B1)] is

$$\begin{aligned}\boldsymbol{S} &= \frac{1}{\mu_0}\boldsymbol{\mathcal{E}}\times\boldsymbol{\mathcal{B}} \\ &= \frac{\mu^2}{4\pi\alpha}k_0^2(m_e c^2)^2\{[f_1'(k\cdot x)]^2 + [f_2'(k\cdot x)]^2\}\boldsymbol{n},\end{aligned} \tag{B7}$$

where $\mu_0$ is the vacuum magnetic permeability, and where we have introduced the relativistically invariant parameter $\mu$, defined according to Eq. (54). The shape functions will be always normalized such that

$$\frac{1}{2\pi}\int_0^{2\pi} d\phi\{[f_1'(\phi)]^2 + [f_2'(\phi)]^2\} = \frac{1}{2}, \tag{B8}$$

which corresponds to the normalization of a plane wave field. Thus, the pulse-averaged intensity becomes

$$I = \frac{\mu^2}{8\pi\alpha}k_0^2(m_e c^2)^2. \tag{B9}$$

If the laser pulse contains $N_{\rm osc}$ oscillations of the field, its central frequency is $\omega_{\rm L} = N_{\rm osc}ck_0$. Therefore,

$$I = \frac{\omega_{\rm L}^2(m_e c)^2}{8\pi\alpha}\left(\frac{\mu}{N_{\rm osc}}\right)^2. \tag{B10}$$

In the case considered in Secs. III, IV, and V, we choose $f_1(\phi) = Bf(\phi)$ and $f_2(\phi) = 0$. Keeping the normalization of the shape function,

$$\frac{1}{2\pi}\int_0^{2\pi} d\phi[f'(\phi)]^2 = \frac{1}{2}, \tag{B11}$$

we find from Eq. (B10) that

$$I = \frac{\omega_{\rm L}^2(m_e c)^2}{8\pi\alpha}\left(\frac{\mu B}{N_{\rm osc}}\right)^2. \tag{B12}$$

As one can see, if for a fixed frequency of the pulse, $\omega_{\rm L}$, and for a fixed intensity, $I$, we would like to compare the pair creation signal for different pulse durations, we should choose $B = N_{\rm osc}$.


[1] H. R. Reiss, J. Math. Phys. **3**, 59 (1962).
[2] A. I. Nikishov and V. I. Ritus, Zh. Eksp. Teor. Fiz. **46**, 776 (1964) [Sov. Phys. JETP **19**, 529 (1964)].
[3] V. P. Yakovlev, Zh. Eksp. Teor. Fiz. **49**, 318 (1965) [Sov. Phys. JETP **22**, 223 (1966)].
[4] See the ELI proposal on http://www.extreme-light-infrastructure.eu.
[5] F. Ehlotzky, K. Krajewska, and J. Z. Kamiński, Rep. Prog. Phys. **72**, 046401 (2009).
[6] A. Di Piazza, C. Müller, K. Z. Hatsagortsyan, and C. H. Keitel, Rev. Mod. Phys. **84**, 1177 (2012).
[7] D. Burke *et al.*, Phys. Rev. Lett. **79**, 1626 (1997).
[8] C. Müller, A. B. Voitkiv, and N. Grün, Phys. Rev. A **67**, 063407 (2003).
[9] P. Sieczka, K. Krajewska, J. Z. Kamiński, P. Panek, and F. Ehlotzky, Phys. Rev. A **73**, 053409 (2006).
[10] A. I. Milstein, C. Müller, K. Z. Hatsagortsyan, U. D. Jentschura, and C. H. Keitel, Phys. Rev. A **73**, 062106 (2006).
[11] J. Z. Kamiński, K. Krajewska, and F. Ehlotzky, Phys. Rev. A **74**, 033402 (2006).
[12] M. Y. Kuchiev and D. J. Robinson, Phys. Rev. A **76**, 012107 (2007).
[13] A. Di Piazza and A. I. Milstein, Phys. Lett. B **717**, 224 (2012).
[14] C. Müller, A. B. Voitkiv, and N. Grün, Phys. Rev. Lett. **91**, 223601 (2003).
[15] S. J. Müller and C. Müller, Phys. Rev. D **80**, 053014 (2009).
[16] K. Krajewska and J. Z. Kamiński, Phys. Rev. A **82**, 013420 (2010).
[17] K. Krajewska and J. Z. Kamiński, Phys. Rev. A **84**, 033416 (2011).
[18] K. Krajewska, Laser Phys. **21**, 1275 (2011).
[19] T.-O. Müller and C. Müller, Phys. Lett. B **696**, 201 (2011); Phys. Rev. A **86**, 022109 (2012).
[20] A. Di Piazza, A. I. Milstein, and C. Müller, Phys. Rev. A **82**, 062110 (2010).
[21] E. Lötstedt, U. D. Jentschura, and C. H. Keitel, New J. Phys. **11**, 013054 (2009).
[22] A. Di Piazza, E. Lötstedt, A. I. Milstein, and C. H. Keitel, Phys. Rev. A **81**, 062122 (2010).
[23] K. Krajewska and J. Z. Kamiński, Phys. Rev. A **85**, 043404 (2012).
[24] K. Krajewska and J. Z. Kamiński, Phys. Rev. A **86**, 021402(R) (2012).
[25] A. A. Lebed' and S. P. Roshchupkin, Laser Phys. **21**, 1613 (2011); S. P. Roshchupkin, A. A. Lebed', E. A. Padusenko, and A. I. Voroshilo, *ibid.* **22**, 1113 (2012); S. P. Roshchupkin, A. A. Lebed', and E. A. Padusenko, *ibid.* **22**, 1513 (2012).

[26] M. Boca and V. Florescu, Phys. Rev. A **80**, 053403 (2009); Eur. Phys. J. D **61**, 449 (2011); M. Boca, V. Dinu, and V. Florescu, Phys. Rev. A **86**, 013414 (2012).
[27] T. Heinzl, D. Seipt, and B. Kämpfer, Phys. Rev. A **81**, 022125 (2010); D. Seipt and B. Kämpfer, *ibid.* **83**, 022101 (2011).
[28] F. Mackenroth, A. Di Piazza, and C. H. Keitel, Phys. Rev. Lett. **105**, 063903 (2010); F. Mackenroth and A. Di Piazza, Phys. Rev. A **83**, 032106 (2011).
[29] A. I. Voroshilo, S. P. Roshchupkin, and V. N. Nedoreshta, Laser Phys. **21**, 1675 (2011).
[30] D. Seipt and B. Kämpfer, Phys. Rev. D **85**, 101701(R) (2012).
[31] K. Krajewska and J. Z. Kamiński, Phys. Rev. A **85**, 062102 (2012).
[32] T. Heinzl, A. Ilderton, and M. Marklund, Phys. Lett. B **692**, 250 (2010).
[33] A. I. Titov, H. Takabe, B. Kämpfer, and A. Hosaka, Phys. Rev. Lett. **108**, 240406 (2012).
[34] K. Krajewska and J. Z. Kamiński, Phys. Rev. A **86**, 052104 (2012).
[35] A. Ipp, J. Evers, C. H. Keitel, and K. Z. Hatsagortsyan, Phys. Lett. B **702**, 383 (2011).
[36] M. V. Fedorov, M. A. Efremov, and P. A. Volkov, Opt. Commun. **264**, 413 (2006).
[37] M. Ruf, G. R. Mocken, C. Müller, K. Z. Hatsagortsyan, and C. H. Keitel, Phys. Rev. Lett. **102**, 080402 (2009).
[38] F. Hebenstreit, R. Alkofer, G. V. Dunne, and H. Gies, Phys. Rev. Lett. **102**, 150404 (2009); C. K. Dumlu and G. V. Dunne, *ibid.* **104**, 250402 (2010).
[39] M. Jiang, W. Su, Z. Q. Lv, X. Lu, Y. J. Li, R. Grobe, and Q. Su, Phys. Rev. A **85**, 033408 (2012).
[40] Q. Su, W. Su, Z. Q. Lv, M. Jiang, X. Lu, Z. M. Sheng, and R. Grobe, Phys. Rev. Lett. **109**, 253202 (2012).
[41] N. Ren, J. X. Wang, A. K. Li, and P. X. Wang, Chin. Phys. Lett. **29**, 071201 (2012).
[42] O. P. Novak and R. I. Kholodov, Phys. Rev. D **86**, 105013 (2012).
[43] F. Fillion-Gourdeau, E. Lorin, and A. D. Bandrauk, Phys. Rev. Lett. **110**, 013002 (2013).
[44] H. Chen, S.C. Wilks, J.D. Bonlie, E.P. Liang, J. Myatt, D.F. Price, D.D. Meyerhofer, and P. Beiersdorfer, Phys. Rev. Lett. **102**, 105001 (2009).
[45] V. S. Popov, Zh. Eksp. Teor. Fiz. **63**, 1586 (1972) [Sov. Phys. JETP **36**, 840 (1973)].
[46] D. B. Milošević, G. G. Paulus, D. Bauer, and W. Becker, J. Phys. B **39**, R203 (2006).
[47] M. Klaiber, K. Z. Hatsagortsyan, and C. H. Keitel, Phys. Rev. A **75**, 063413 (2007); M. Klaiber, E. Yakaboylu, and K. Z. Hatsagortsyan, *ibid.* **87**, 023418 (2013).
[48] A. D. DiChiara, I. Ghebregziabher, R. Sauer, J. Waesche, S. Palaniyappan, B. L. Wen, and B. C. Walker, Phys. Rev. Lett. **101**, 173002 (2008).
[49] F. H. M. Faisal and S. Bhattacharyya, Phys. Rev. Lett. **93**, 053002 (2004).
[50] Spin effects have recently also been studied with respect to other related processes in external fields; see, e.g., O. P. Novak and R. I. Kholodov, Phys. Rev. D **80**, 025025 (2009); T. Cheng, M. R. Ware, Q. Su, and R. Grobe, Phys. Rev. A **80**, 062105 (2009); D. V. Karlovets, *ibid.* **84**, 062116 (2011).
[51] F. Dreisow, S. Longhi, S. Nolte, A. Tünnermann, and A. Szameit, Phys. Rev. Lett. **109**, 110401 (2012).
[52] R. A. Neville and F. Rohrlich, Phys. Rev. D **3**, 1692 (1971).
[53] D. M. Volkov, Z. Phys. **94**, 250 (1935).
[54] C. Itzykson and J.-B. Zuber, *Quantum Field Theory* (McGraw-Hill, New York, 1980).
[55] B. Borca, M. V. Frolov, N. L. Manakov, and A. F. Starace, Phys. Rev. Lett. **88**, 193001 (2002).
[56] K. Krajewska, I. I. Fabrikant, and A. F. Starace, Phys. Rev. A **74**, 053407 (2006); **78**, 023407 (2008); **86**, 053410 (2012).